JOURNAL OF MATERIALS SCIENCE 30 (1995) 2325–2329

Reactive deposition of tungsten and titanium carbides by induction plasma

X. L. JIANG, F. GITZHOFER, M. I. BOULOS
Plasma Technology Research Center, Department of Chemical Engineering, University of Sherbrooke, Sherbrooke, PQ J1K 2R1 Canada

R. TIWARI
Department of Chemical Engineering, Cleveland State University, Cleveland, OH 44115 USA

A study is reported on the use of induction plasma technology for the preparation of dense free-standing deposits of tungsten carbide and titanium carbide from metallic powders and methane. Phase analysis by X-ray diffraction indicates that primary carburization of the particles takes place in-flight giving rise to the formation of W_2C and TiC_{1-x}. Secondary carburization occurs in the deposits resulting in the formation of tungsten and titanium carbides. Microstructures revealed by optical and scanning electron microscopy show uniform small grains of the carbides. The reactive plasma spray-formed tungsten carbide shows transgranular fracture, while pure tungsten deposits show intergranular fracture.

1. Introduction

Carbides have a unique set of properties necessary for many applications such as cutting tools and dies. These properties include great hardness and wear resistance, good thermal shock resistance and thermal conductivity, and good oxidation resistance. Current commercial processes to form tungsten carbide involve heating stoichiometrically mixed fine powders of elemental tungsten and carbon in an oven at a temperature of 1773 K until the reaction (W + C = WC) is complete. A disadvantage of the long processing time can be seen in the relatively course grain size of the tungsten carbide product. It has been determined that shorter reaction time reduces grain growth, thus producing smaller grain size which, in turn, aids the overall strength and toughness of the final product [1].

Production of tungsten carbide by the vapour-phase reaction of tungsten halide, e.g. tungsten hexacholoride, with a carbon source, e.g., methane, in the presence of hydrogen, has been described [2]. The principal product obtained by the vapour-phase route is ditungsten carbide (W_2C). Subsequent heating at 1273 K for about 1–2 h is required to make a product with tungsten carbide (WC) as a principal phase.

Recently, reactive spray synthesis in d.c. plasma has been used to form WC/W and TiC/Ti composites [3, 4]. These composites contain limited fraction of carbides. The carbide particles are embedded in a tough metallic matrix where the carbides act as bearing for the sliding surface, reducing friction coefficients, preventing adhesive metal transfer so that the wear resistance is improved. A definite amount of oxides and porosity is also present in these composites.

Induction plasma processing of materials has been widely accepted over the past ten years for applications such as crystal growth, powder spheroidization, coatings, sintering, and chemical synthesis [5–11]. The inherent characteristics of induction plasma for reactive spray forming are the absence of electrodes, the ability for axial injection of the reactants and the long residence time of the order of 10–25 ms. These characteristics are particularly useful in the complete melting of large feedstock particles and for the in-flight chemical reactions.

In our previous studies [12–14], it has been demonstrated that the induction plasma spraying is an attractive spray-forming technology for tungsten metal processing. In this study, induction plasma spraying is used to obtain free-standing deposits of tungsten carbide and titanium carbide from metallic powders and methane by plasma reactive deposition.

2. Experimental procedure

Plasma reactive deposition was performed using our 50 kW, 3 MHz induction plasma facility. A schematic drawing of the experimental apparatus is given in Fig. 1. It consisted of a high-energy density torch operated with pure argon as the central gas and argon–hydrogen mixture as sheath gas. The precursor powder was axially injected into the plasma discharge using a water-cooled stainless steel probe positioned at the centre of the induction coil. The exit of the torch was connected to a water-cooled stainless steel vacuum chamber.

The tungsten powder feedstock, obtained from Sylvania, Chemicals and Metals, Towanda, USA, has a mean particle size of 5 μm. Titanium powder from Sultzer Plasma-Technik has a particle size range of 45–90 μm. The reactive deposition conditions are summarized in Table I. Tungsten carbide deposits

0022–2461

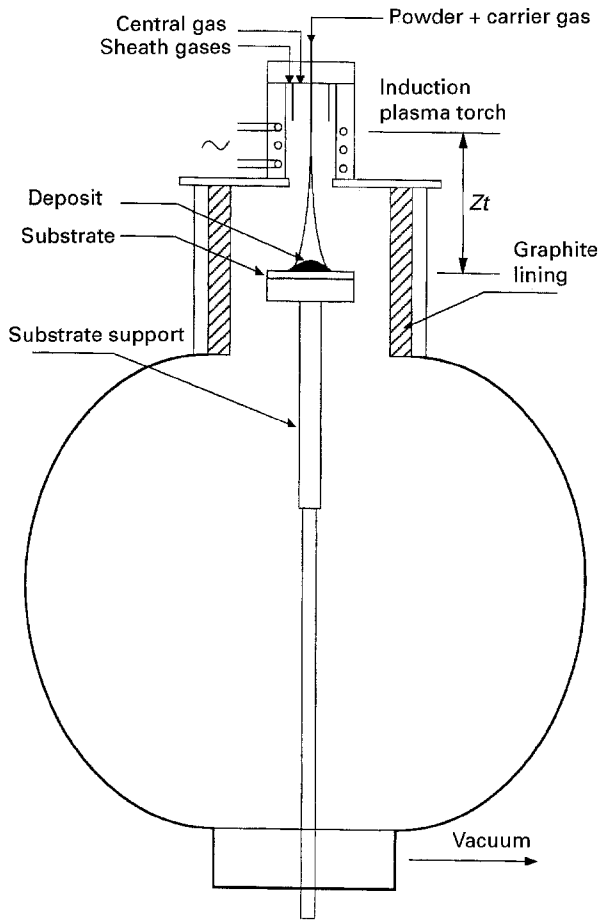

Figure 1 Schematic drawing of the experimental apparatus used for the creative deposition; Zt = spray distance.

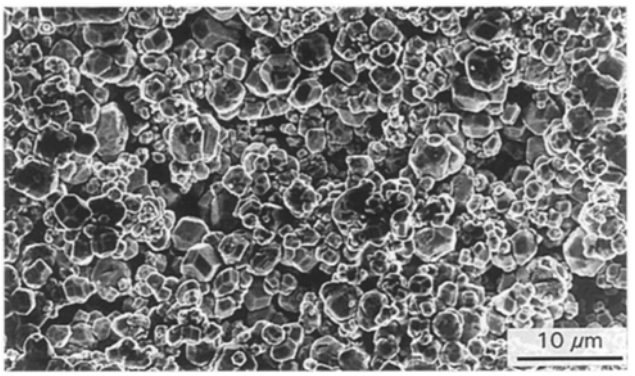

Figure 2 Scanning electron micrograph of the original tungsten powder.

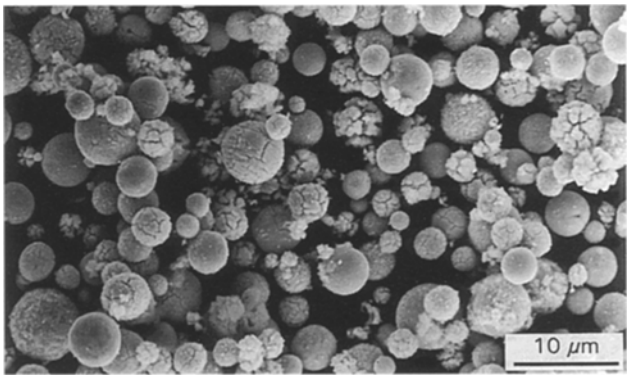

Figure 3 Scanning electron micrograph of the reactive plasma-processed powder; 4.2 standard $l\,min^{-1}$ (CH_4), 10 $g\,min^{-1}$ (W), 50 kW, 200 torr.

were obtained on stationary graphite substrates which were pre-coated with a thin layer of boron nitride aerosol to enable removal of the deposits after reactive deposition. X-ray diffraction analysis was conducted on a Rigaku Geigerflex unit, using CuK_α radiation. Optical and scanning electron microscopy was used for microstructural examinations. Microhardness measurements were performed on a Buehler Microhardness Tester, using an 0.3 kg indentation load.

3. Results and discussion

3.1. Phase analysis and reaction mechanisms

3.1.1. Tungsten carbides

Electron micrographs of the tungsten powder feedstock used and the powder obtained by plasma reactive processing are given in Figs 2 and 3, respectively. The later powder was collected in a cold steel basin at a spray distance of 450 mm. The operating conditions were 10 $g\,min^{-1}$ powder feeding and 4.2 standard $l\,min^{-1}$ methane flow. The mole ratio of C/W is 3.5.

It can be seen from Fig. 3 that all of the particles have been melted and spheroidized. The particle surfaces are rough and some particles have cracked surfaces. The X-ray diffraction pattern shown in Fig. 4 reveals the presence of two major constituent phases, W_2C and pure tungsten. The spheroidization results show that there was insignificant vaporization of the powder.

The thermodynamic equilibrium diagram (Fig. 5) shows that CH_4 decomposes at about 1000 K and that there is solid carbon available near the melting temperature of tungsten. As shown in Fig. 3, the carbon was condensed on the particle surfaces. X-ray diffraction

TABLE I Reactive deposition conditions

Parameters	Tungsten carbide	Titanium carbide
Sheath gas	90 standard $l\,min^{-1}(Ar)^+$ 9 standard $l\,min^{-1}(H_2)$	90 standard $l\,min^{-1}(Ar)^+$ 9 standard $l\,min^{-1}(H_2)$
Central gas	40 standard $l\,min^{-1}(Ar)$	40 standard $l\,min^{-1}(Ar)$
Carrier gas	2–17 standard $l\,min^{-1}(CH_4)$	2 standard $l\,min^{-1}(CH_4)$
Particle size	5–60 μm	45–90 μm
Powder feed rate	10–40 $g\,min^{-1}$	5 $g\,min^{-1}$
Power level	35–50 kW	50 kW
Reactor pressure	200–400 torr	200 torr
Spray distance	200–450 mm	200–450 mm

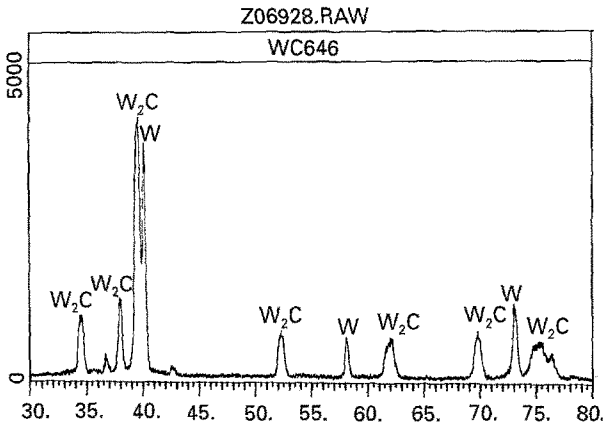

Figure 4 X-ray diffraction pattern of the powder shown in Fig. 3.

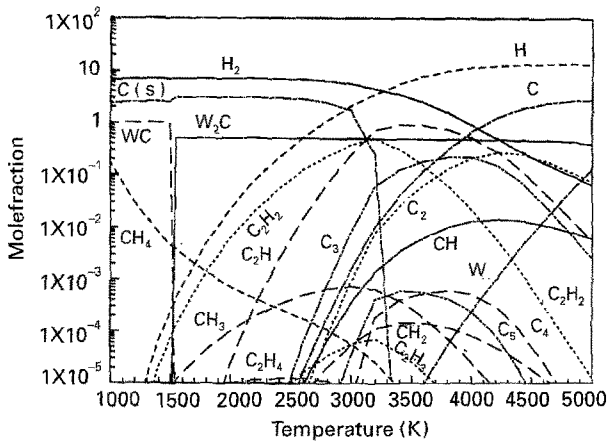

Figure 5 Thermodynamic equilibrium diagram for the C–H–W system; 4.2 standard l min^{-1} (CH_4), 10 g min^{-1} (W), 200 torr.

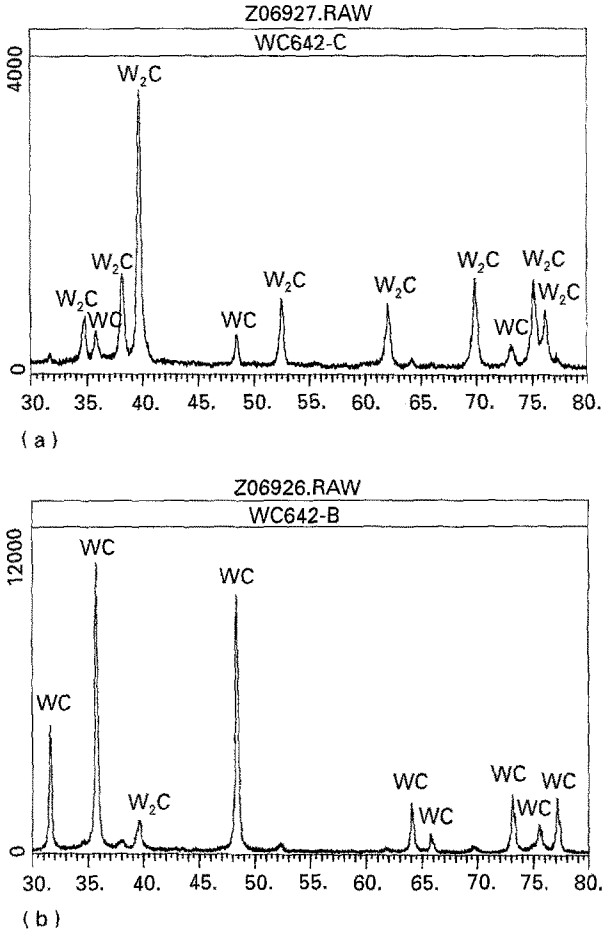

Figure 6 X-ray diffraction patterns of a tungsten carbide deposit; 4.2 standard l min^{-1} (CH_4), 10 g min^{-1} (W), 50 kW, 200 torr: (a) deposit centre, (b) deposit bottom.

analysis of the reactive plasma-processed powder shows that a primary carburization which occurred in-flight gives a typical 60% W_2C concentration under the conditions of 3.5 CH_4/W molar ratio and 200 torr (1 torr = 133.322 Pa) reactor pressure.

Considering that the diffusion-controlled reaction rate depends exponentially on temperature, and the diffusion coefficient in a liquid is much higher than in a solid, significant carburization of the particles in-flight will begin when the particles are in a molten state. The principal reactions involved in the process are

$$CH_4(g) = C(s) + 2H_2(g) \quad (1)$$

$$C(s) + 2W(l) = W_2C(l) \quad (2)$$

As shown in Fig. 6, the X-ray diffraction analysis of the deposits indicates that the deposit consists exclusively of W_2C/WC with no pure tungsten present. The ratio of W_2C to WC is noted to change between the middle and bottom sections of the deposit. The highest concentration of WC being present in the deposit bottom could be due to reaction with carbon on the graphite substrate and due to the fact that the bottom layer had the largest exposure time to the plasma. The substrate temperature was measured during the deposition process as 2100 K at 200 mm spray distance. It is evident that secondary carburization has occurred on the substrate at such a temperature. The necessary solid carbon for the secondary carburization to occur comes from the high carbon to tungsten molar ratio (3.5). Under the impact of the falling particles, the lamellae develop and are exposed to a larger surface of carbon so that the carburization process continues. Finally, all of the tungsten metal is carburized. The thermodynamic stable phase of W_2C will transform into WC when sufficient carbon is available. The following reactions are likely to take place during the deposit formation on the substrate

$$2W(s) + C(s) = W_2C(s) \quad (3)$$

$$W_2C(s) + C(s) = 2WC(s) \quad (4)$$

3.1.2. Titanium carbide

Similar reactions could exist in the plasma reactive deposition of titanium carbide. The primary in-flight carburization of titanium particles gives rise to the formation of TiC_{1-x} according to the following reaction

$$(1-x)C(s) + Ti(l) = TiC_{1-x}(l) \quad (5)$$

The secondary carburization of the deposit on the substrate leads to the complete carburization of titanium (Fig. 7) and the transformation from TiC_{1-x} to TiC according to the reactions

$$Ti(s) + (1-x)C(s) = TiC_{1-x}(s) \quad (6)$$

$$TiC_{1-x}(S) + xC(s) = TiC(s) \quad (7)$$

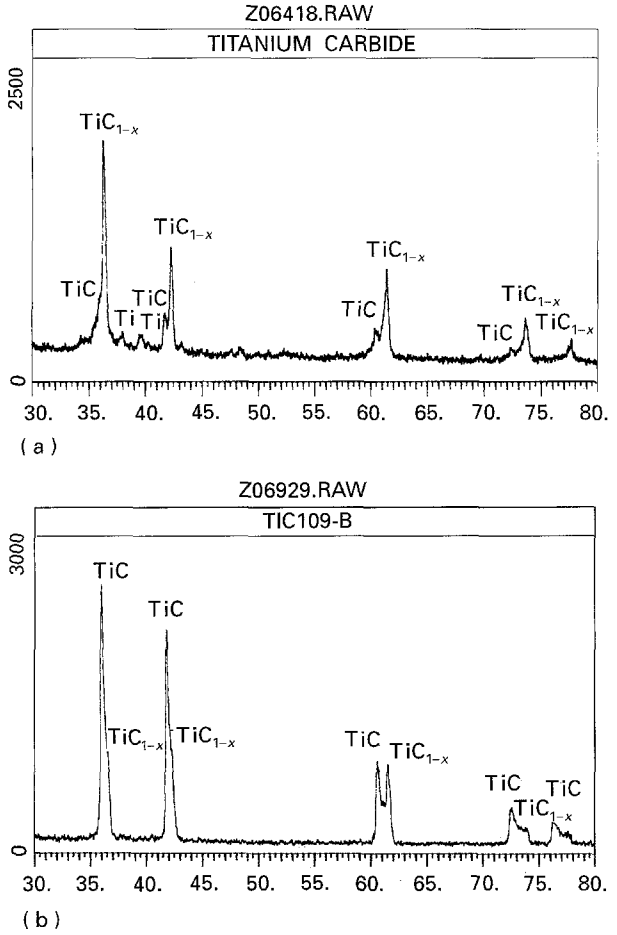

Figure 7 X-ray diffraction patterns of a titanium carbide deposit: (a) deposit centre, (b) deposit bottom.

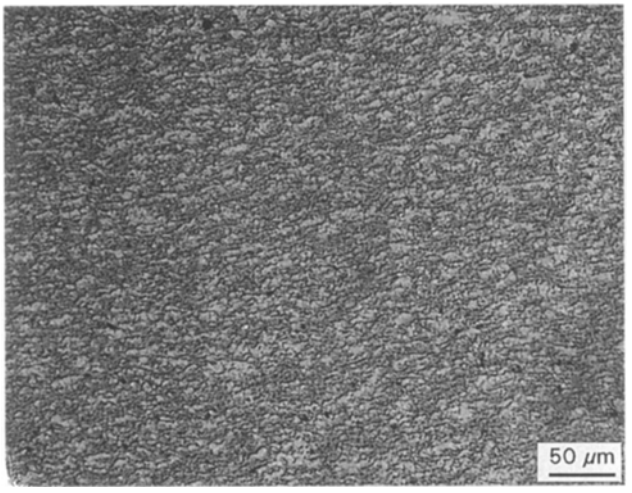

Figure 8 Optical micrograph of a tungsten carbide deposit under the same conditions as in Fig. 6.

3.2. Microstructure characterization

The optical micrograph of the cross-section for a tungsten carbide deposit reveals a microstructure consisting of small uniform grains as shown in Fig. 8. Average grain size was measured to be 3 μm, which is much smaller than that of pure tungsten deposits. The equiaxed grains of the carbides, instead of a lamellar structure, indicates grain growth after the formation of the deposit. The process is, however, inhibited by the presence of the carbon. Because the X-ray diffraction

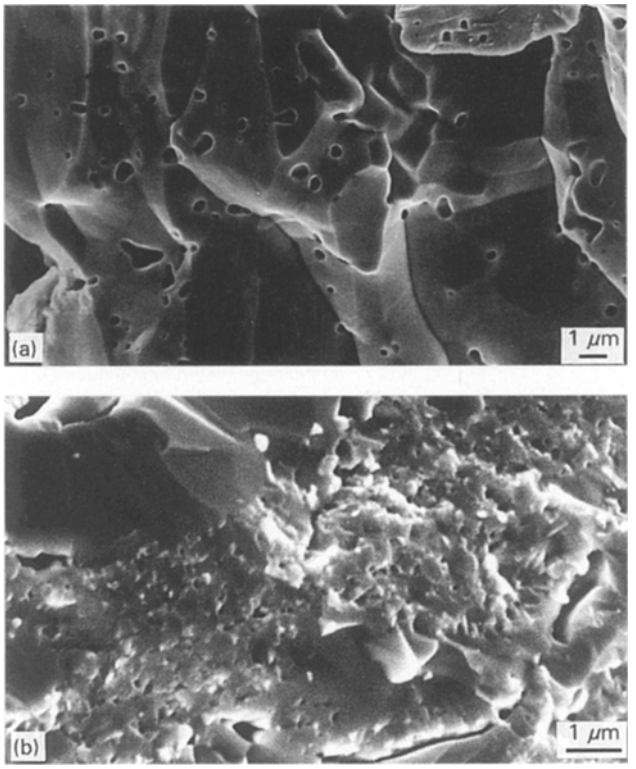

Figure 9 Electron micrographs of deposit fracture surfaces: (a) pure tungsten, (b) tungsten carbide.

result has shown 91% W_2C and 9% WC in the sample centre, the equiaxed grains on the electron micrograph shown in Fig. 8 should be W_2C, whereas the grain or lamellar structure should be WC phase.

The deposit density for tungsten carbide was measured to be 16 000 $kg\,m^{-3}$. Image analysis revealed about 4% porosity in the carbide deposits. Compared to the bottom layer, slightly more porosity can be found at the deposit top, which is typical of the thermal spraying process. The microhardness of the samples was 2140 VHN, which is much higher than that of pure tungsten deposits (430 VHN). Because the W_2C phase is harder than tungsten, and the WC phase is harder than W_2C, the microhardness is directly proportional to the carbide content. It was found that both pure tungsten deposits and carbide deposits show brittle rupture, but the fracture behaves in different ways. Pure tungsten deposits show intergranular fracture (Fig. 9), indicating a weakness among large grains, while tungsten carbide under an identical fabrication condition demonstrates transgranular fracture, reflecting the high strength of the material.

The microstructure of the reactive plasma spray-formed titanium carbide is shown in Fig. 10. The deposit density was measured to be 4730 $kg\,m^{-3}$. Image analysis on the microstructure revealed 3.0% porosity. Microhardness was 1990 VHN. It should be pointed out that the titanium carbide will spall or crack during fast cooling.

4. Conclusions

Induction plasma spraying has been successfully utilized for reactive spray-forming of tungsten carbide and titanium carbide. Dense free-standing deposits

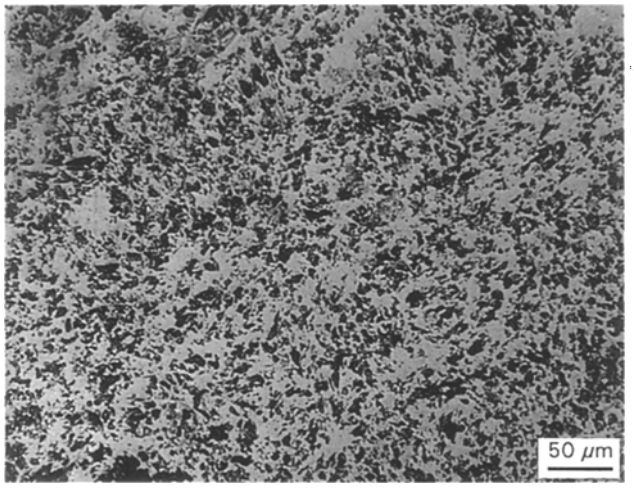

Figure 10 Optical micrograph of a titanium carbide deposit.

have been synthesized from metallic powder and methane in a single step. Methane, used as carrier gas, ensures the full contact of reactants and increases reaction possibility and homogeneity both in-flight and on the deposits.

The primary carburization of the particles takes place in-flight through the reaction of the molten droplets with methane, resulting in the formation of W_2C or TiC_{1-x}. The secondary carburization which takes place in the deposits is a solid–solid reaction, resulting in the complete formation of carbides and the phase transformations from W_2C to WC and from TiC_{1-x} to TiC. The carbide deposits formed by the reactive plasma spray have a uniform microstructure consisting of small grains. Tungsten carbide deposits show the transgranular fracture, whereas pure tungsten deposits show intergranular fracture.

Acknowledgements

This project was partially supported by a grant from the Ministere de l'Énergie et des Ressources du Quebéc. The financial support by the Ministere de l'Éducation de la Province de Québec through its FCAR programme and the Natural Sciences and Engineering Research Council of Canada is gratefully acknowledged.

References

1. R. H. CHURCH, J. B. SALSMAN and B. J. HAMNER, US Pat. 5 131 992 (1992).
2. R. A. STEIGER, C. FULTON and W. L. WILSON, US Pat. 3848 062 (1974).
3. R. W. SMITH and Z. Z. MUTASIM, *J. Thermal Spray Tech.* **1** (1992) 57.
4. R. W. SMITH, *Powder Metall. Int.* **25** (1993) 9.
5. M. I. BOULOS, *Pure Appl. Chem.* **57** (1985) 1321.
6. J. JUREWICZ, R. KACZMAREK and M. I. BOULOS, in "Proceedings of the 7th International Symposium on Plasma Chemistry", edited by C. Timmermans, Eindhoven, Vol. **4** (1985) p. 1131.
7. M. I. BOULOS and J. JUREWICZ, US Pat. 4853 250 (1989).
8. S. TAKEUCHI, T. OKADA, T. YOSHIDA and K. AKASHI, in "Proceedings of the 8th International Symposium on Plasma Chemistry", edited by K. Akashi and A. Kinbara, Tokyo, Vol. **4** (1987) p. 1928.
9. S. TAKEUCHI, T. OKADA, T. YOSHIDA and K. AKASHI, *J. Jpn Inst. Metals* **52** (1988) 711.
10. C. B. LAFLAMME, G. SOUCY, J. W. JUREWICZ and M. I. BOULOS, *High Temp. Chem. Process.* **1** (1992) 283.
11. T. ISHIGAKI, T. TAKANA, T. SATO, Y. MORIYOSHI and M. I. BOULOS, in "Proceedings of Japanese Symposium on Plasma Chemistry", edited by C. Bemdt and T. Bemecki Vol. 5 (ASM, Materials Park, Ohio, 1992) p. 251.
12. X. L. JIANG, X. B. FAN, F. GITZHOFER and M. I. BOULOS, in "Proceedings of the 13th International Thermal Spray Conference", edited by C. Bemdt Orlando, 28 May–5 June (ASM, Materials Park, Ohio, 1992) p. 39.
13. X. L. JIANG, R. TIWARI, F. GITZHOFER and M. I. BOULOS, in "Proceedings of the 5th National Thermal Spray Conference", edited by A. Matsuda, Y. Horüke, T. Mariyoshi and K. Takeda Anaheim, 7–11 June (Tokyo, 1993) p. 309.
14. X. L. JIANG, R. TIWARI, F. GITZHOFER and M. I. BOULOS, *J. Thermal Spray Tech.* **2** (1993) 265.

Received 15 February
and accepted 4 October 1994